

# U-Pb Dating of Large Zircons in Low-Temperature Jadeitite from the Osayama Serpentinite Mélange, Southwest Japan: Insights into the Timing of Serpentinization

T. TSUJIMORI,<sup>1</sup> J. G. LIU,

*Department of Geological and Environmental Sciences, Stanford University, Stanford, California 94305*

J. WOODEN,

*United States Geological Survey, 345 Middlefield Road, Menlo Park, California 94025*

AND T. MIYAMOTO

*Department of Earth and Planetary Sciences, Faculty of Sciences, Kyushu University, Fukuoka, 812-8581, Japan*

## Abstract

Crystals of zircon up to 3 mm in length occur in jadeitite veins in the Osayama serpentinite mélange, Southwest Japan. The zircon porphyroblasts show pronounced zoning, and are characterized by both low Th/U ratios (0.2–0.8) and low Th and U abundances (Th = 1–81 ppm; U = 6–149 ppm). They contain inclusions of high-pressure minerals, including jadeite and rutile; such an occurrence indicates that the zircon crystallized during subduction-zone metamorphism. Phase equilibria and the existing fluid-inclusion data constrain P-T conditions to  $P > 1.2$  GPa at  $T < 350^\circ\text{C}$  for formation of the jadeitite. Most U/Pb ages obtained by SHRIMP-RG are concordant, with a weighted mean  $^{206}\text{Pb}/^{238}\text{U}$  age of  $472 \pm 8.5$  Ma (MSWD = 2.7,  $n = 25$ ). Because zircon porphyroblasts contain inclusions of high-pressure minerals, the SHRIMP U-Pb age represents the timing of jadeitite formation, i.e., the timing of interaction between alkaline fluid and ultramafic rocks in a subduction zone. Although this dating does not provide a direct time constraint for serpentinization, U-Pb ages of zircon in jadeitite associated with serpentinite result in new insights into the timing of fluid-rock interaction of ultramafic rocks at a subduction zone and the minimum age for serpentinization.

## Introduction

ZIRCON OCCURS as an accessory phase in igneous and metamorphic rocks and is the best mineral for U-Pb age dating, with a closure temperature around  $900^\circ\text{C}$  (Cherniak and Watson, 2001). On the other hand, in low-temperature (LT) environments such as blueschist- and greenschist-facies conditions, new zircon growth and overgrowth are very rare. Hence U-Pb dating of zircon in subduction-zone metamorphic rocks has been very limited. However, crystallization of zircon from hydrothermal fluid has been documented (e.g., Rubin et al., 1989; Rubatto and Hermann, 2003). In such LT environments, hydrothermal fluid may cause partial dissolution of pre-existing zircon and precipitation of neoblastic zircon (e.g., Hansen and Friderichsen, 1989; Sinha et al., 1992; Vavra et al., 1999). These processes accom-

pany Pb or U loss and cause isotopic discordance at LT conditions.

Serpentinite is a unique environment for precipitation of hydrothermal zircon. Zircon has been reported from serpentinite-related LT metasomatic rocks such as rodingite blackwall and jadeitite (Kobayashi et al., 1987; Harlow, 1994; Bröcker and Enders, 1999; Miyajima et al. 2001; Dubińska et al. 2004); reconnaissance U-Pb dating for such LT zircon has just began (e.g., Bröcker and Enders, 1999; Kunugiza et al., 2002; Dubinska et al., 2004). Isotopic and chemical information on these zircon crystals provide a key not only to understand the fluid history concerning serpentinization but also to evaluate the hydrothermal effects on both growth and dissolution of zircon at LT conditions.

In this contribution, we present SHRIMP (sensitive, high-resolution ion microprobe) U-Pb isotopic data for large hydrothermal zircon crystals, up to 3 mm in size, in jadeitite (nearly monomineralic

<sup>1</sup>Corresponding author; email: tatsukix@pangea.stanford.edu

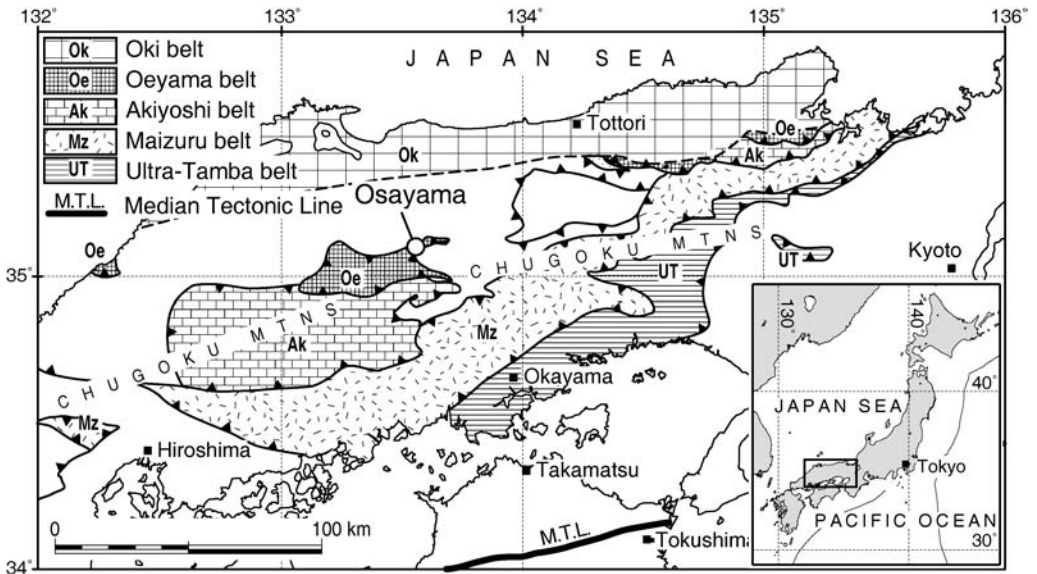


FIG. 1. Simplified map of the Chugoku Mountains of Southwest Japan, showing various pre-Triassic geotectonic units and the sample locality.

jadeite-rich rock) from a serpentinite-matrix mélangé in the Osayama Mountain, Southwest Japan. Although zircon porphyroblasts from this locality have been previously considered as a relict igneous phase (Miyamoto and Yanagi, 1998), we have recently found a few jadeite inclusions in zircon. We also describe the internal texture and U-Th chemistry of hydrothermal zircon, discuss the implications for the zircon crystallization in jadeite, and comment on the U-Pb age dating for serpentinitization at a subduction zone.

### Geologic Outline

Jadeitite, omphacitite, albitite, rodingite, and blueschist-facies schist have been identified as blocks in the Osayama serpentinite mélangé of the central Chugoku Mountains (Tsujimori, 1997; Tsujimori and Itaya, 1999; Tsujimori and Liou, 2004a, 2005a, 2005b) (Fig. 1). Serpentinized peridotite bodies and related mélangés occur as an Early Paleozoic ophiolitic nappe that occupies the highest structural position of the Oeyama belt (Ishiwatari and Tsujimori, 2003). Chrysotile and lizardite are major serpentine-group minerals in the Osayama mélangé (Tsujimori, 1998). Protoliths of the serpentinites consist mainly of harzburgite with minor dunite, podiform chromitite, and gabbroic dikes (e.g., Arai, 1980); the

gabbroic intrusives with MORB-like geochemical signatures yield Sm-Nd isochron ages of ca. ~560 Ma (Hayasaka et al., 1995). Phengites from blueschist-facies schists at Osayama yield K-Ar ages of 327–273 Ma (Tsujimori and Itaya, 1999).

Jadeitites in the Osayama serpentinite mélangé occur as veins up to 4 m wide. They are composed mainly of jadeite (generally 75% by volume) with minor amounts of grossular (nearly pure), and trace rutile and zircon. The jadeite-rich matrix is heterogeneous and shows variable degrees of retrogression. Omphacite, analcime, pectolite, stronalsite, thomsonite, natrolite, vesuvianite, prehnite, phlogopite, serpentinite, and titanite are retrograde phases (Kobayashi et al., 1987; Tsujimori, 1998). Shoji and Kobayashi (1988) described primary fluid inclusions in jadeite. Preliminary U-Pb ages of large zircon porphyroblasts in jadeitite using conventional thermal ionization mass spectrometry yield ca. 500–450 Ma (Miyamoto and Yanagi, 1998); the data was interpreted as the crystallization age of an igneous protolith for the jadeitite.

### Sample Description and Condition of Zircon Crystallization

Electron microprobe analysis for rock-forming minerals was carried out with a JEOL JXA-8900R at

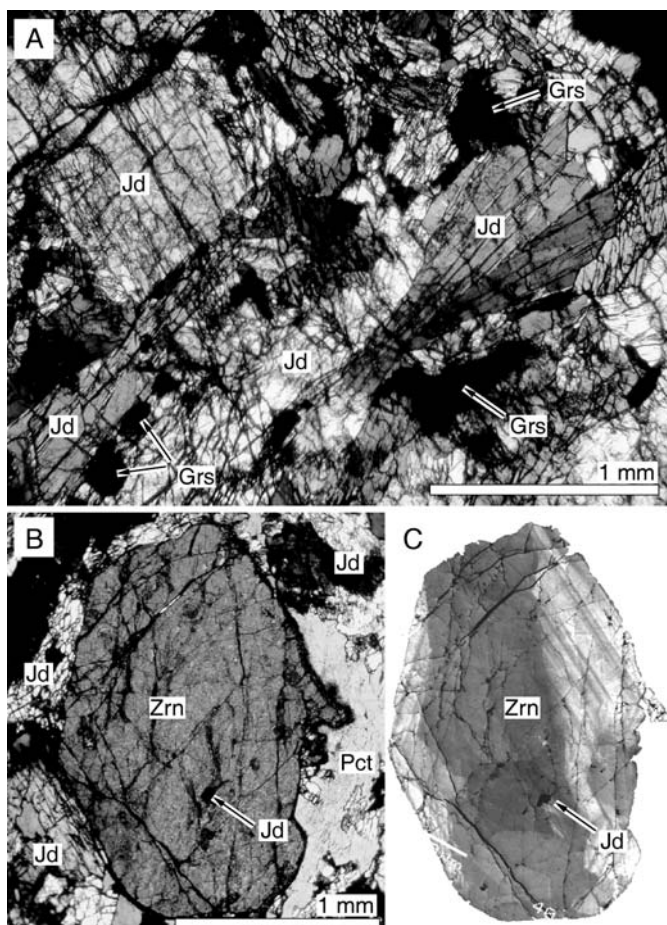


FIG. 2. Microtexture of the investigated jadeite. A. Plane polarizer view of the occurrence of jadeite (Jd) with grossular (Grs). B. Plane polarizer view of occurrences of zircon (Zrn); matrix minerals including jadeite (Jd) and secondary pectolite (Pct) are also shown. C. Cathodoluminescence image of zircon of (B). Texture shows zircon consisting of at least two crystals.

Okayama University of Science. Quantitative analyses were performed with 15 kV accelerating voltage, 12 nA beam current, and a 3  $\mu\text{m}$  beam size. The ZAF (oxide basis) method was employed for matrix corrections. Cathodoluminescence (CL) imaging was obtained using a JEOL 5600LV Scanning Electron Microscope (SEM) equipped with a HAMAMATSU photo multiplier tube at Stanford University.

In the investigated sample, jadeite with 91–99 mol%  $\text{NaAl}_2\text{Si}_2\text{O}_6$  (Jd) component occurs as either subhedral to anhedral prismatic crystals or radial aggregates (Figs. 2A and 3); most are less than 0.5 mm in length, but some are up to 5 mm. Jadeite

contains rare grossular, zircon, and rutile as tiny inclusions (< 0.1 mm). Some secondary omphacites (39–58 mol% Jd) epitaxially overgrow jadeite crystals and fill fractures together with analcime (Fig. 3). In the altered sections of the sample, jadeite was extensively replaced by pectolite. Coarse-grained rutile prisms, up to 4 mm long, occur in the jadeite-dominant matrix and are rimmed by secondary titanite that is in contact with secondary pectolite.

Zircon occurs as discrete euhedral to subhedral crystals up to 3 mm in length or as twinned crystals or aggregates in the matrix (Fig. 2B and 2C); zircon contains tiny inclusions of rutile and rare jadeite (97 mol% Jd; Fig. 3). Fine-grained zircon also occurs as

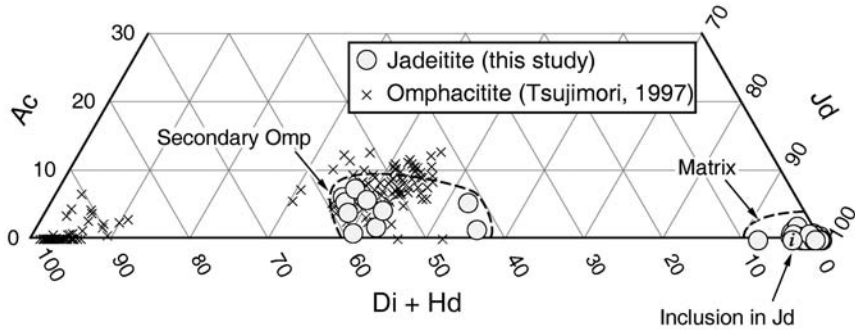


FIG. 3. Compositions of sodic pyroxenes from the investigated jadeitite on the jadeite (Jd)–acmite (Ac)–diopside + hedenburgite (Di + Hd) ternary diagram. The  $\text{Fe}^{2+}/\text{Fe}^{3+}$  ratio for clinopyroxene was estimated assuming a cation total of 4.00.

inclusions in a single jadeite crystal (Kobayashi et al., 1987). This evidence indicates synchronous growth of zircon and jadeite.

Jadeitite formation requires HP condition ( $P > 0.5\text{--}0.6$  GPa at  $T = 200\text{--}400^\circ\text{C}$ ) and infiltration of Na- and Al-rich alkaline fluid (Harlow, 1994; Shi et al., 2003). It is thought that zircon crystals directly crystallized from a hydrothermal fluid during the jadeitite formation in serpentinites. In the Osayama jadeitite, the homogenization  $T$  of fluid inclusions in jadeite examined by Shoji and Kobayashi (1988) requires a minimum of  $\sim 345^\circ\text{C}$  for crystallization of the primary jadeitite minerals. Thermodynamic calculation employing the THERMOCALC program (ver. 3.21) (Powell et al., 1998) indicates  $P > 1.2$  GPa at a nominal  $T = \sim 350^\circ\text{C}$  for the primary jadeite + rutile + grossular assemblage, and  $P = 0.4\text{--}0.6$  GPa at  $200\text{--}300^\circ\text{C}$  for the secondary omphacite + analcime assemblage. The presence of grossular and absence of carbonate minerals suggest low  $X_{\text{CO}_2}$  of the hydrothermal fluid.

### U-Th Chemistry and U-Pb Isotopic Results

U-Th-Pb analyses were performed with the SHRIMP-RG (sensitive high-resolution ion microprobe-reverse geometry) in the Stanford-USGS cooperative ion microprobe facility at Stanford University. Instrumental conditions and data acquisition are similar to the procedures described by Williams (1998). Analytical spots  $\sim 40$   $\mu\text{m}$  in diameter were sputtered using an  $\sim 5$  nA  $\text{O}_2^-$  primary beam. The data were collected in sets of six scans through nine mass spectra. The primary beam was rastered across the analytical spot for 120 s before

analysis to reduce surficial common Pb resulting from sample preparation and Au-coating. Concentration data were calibrated against CZ3 zircon (550 ppm U), and isotope ratios were calibrated against R33 (419 Ma, John Aleinikoff, pers. commun., 2002). Data reduction follows Williams (1998), and utilized Squid (Ludwig, 2001). Isoplot 3 (Ludwig, 2003) was used to calculate all ages, which are reported here at the 95% confidence level.

Representative CL images of three zircon grains are shown in Figure 3; the Th and U abundance from 28 spots of 8 zircon grains are presented in Figure 4. The dating results are shown in Table 1. As shown in the images of Figure 4, zircon porphyroblasts in the Osayama jadeitite have preserved remarkable internal zoning textures including fine, euhedral growth layers with sharp contrasts in CL brightness; these zircons are characterized by low Th and U abundances. Based on textural and geochemical features, analyzed zircons are subdivided into two different zones. Type I is a normal growth zone that is commonly characterized by a broad, stubby core with concentric oscillatory-zoned rims. This texture, shown in Figure 4A, is similar to the growth pattern of hydrothermal zircon crystallized from fluid in serpentinite (e.g., Fig. 7 of Dubińska et al., 2004), and provides evidence of crystallization from fluid. Type I zones in zircon crystals show a wide geochemical variation; Th and U exhibit a positive correlation—Th increases from 3 to 37 ppm as U increases from 11 to 82 ppm. However, concentrations fluctuate greatly from one layer to another (Figs. 4A and 5A). Type II zones in zircon crystals, with dark CL, represent texturally inherited cores rarely preserved in Type I zones (Fig. 4B) and have

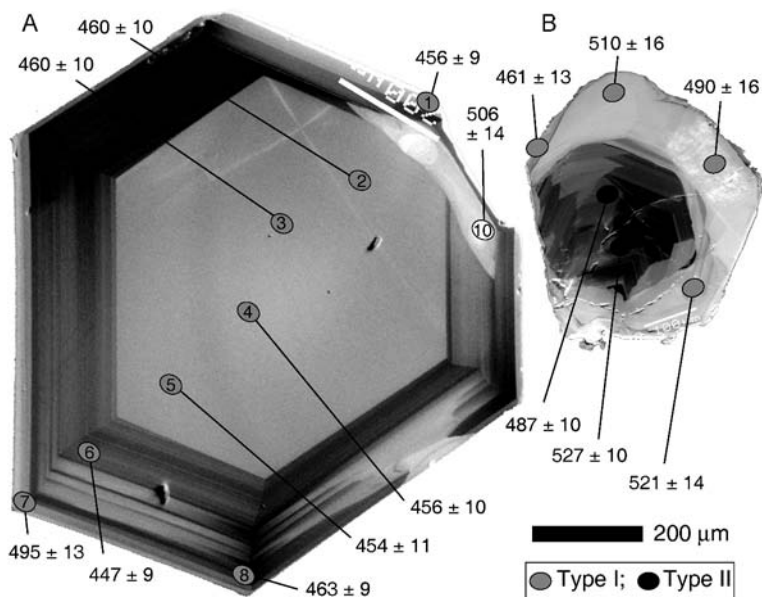


FIG. 4. Cathodoluminescence images of representative zircon separates from the Osayama jadeitite showing growth zoning layers and three zircon zones described in the text. Ellipses within crystal represent primary beam pits; SHRIMP U-Pb results are also shown as apparent  $^{206}\text{Pb}/^{238}\text{U}$  ages (Ma) with  $1\sigma$  errors. For explanation see text. Scale bar represents 200  $\mu\text{m}$ .

very irregular zoning patterns; Th/U ratios of Type II zones are significantly higher (0.70–0.80) than that of the others (0.21–0.48) (Fig. 5B). Textures and different Th/U ratios indicate partial dissolution of early-formed zircon crystals.

The analyzed U-Pb isotopic ratios are plotted on a Tera-Wasserburg diagram with  $1\sigma$  errors (Fig. 6). Most of the data points are concordant within error. Twenty-five analyses of the Type I zone yields  $^{206}\text{Pb}/^{238}\text{U}$  ages arranging 452 to 521 Ma, whereas three analyses of the Type II zone yields 488 to 523 Ma (Table 1). Although the  $^{206}\text{Pb}/^{238}\text{U}$  ages are slightly scattered within the same zones in same zircon crystals (Fig. 4), the lack of noticeable correlation between apparent  $^{206}\text{Pb}/^{238}\text{U}$  age and either U abundance or Th/U ratio (Fig. 5) indicates that the observed chemical variations may not be related to zircon alteration and the U-Pb system may not be significantly disturbed by later events. When the Type II zone is excluded, the type I zone yields a weighted mean  $^{206}\text{Pb}/^{238}\text{U}$  age of  $472 \pm 8.5$  Ma (MSWD = 2.7), which is in agreement with the conventional data (Fig. 6).

### Zircon Growth in Jadeitite from Serpentinite

Most ultramafic rocks contain less than 20 ppm Zr (Erlank et al., 1978); this value is less than 2% of the Zr content of highly evolved granite (>1000 ppm). In fact, zircon in ultramafic rocks is itself very rare except for a few metasomatized peridotites from the Kokchetav Massif, Kazakhstan (e.g., Katayama et al., 2003). Despite such Zr-depleted environments, however, many zircon occurrences in jadeitite and rodingite in serpentinized mantle peridotites have been commonly documented, as mentioned above. On the other hand, formation of nearly monomineralic jadeitite is rare but is almost always restricted to serpentinites from blueschist or eclogite terranes, clearly indicating a subduction-zone environment with a low geotherm (e.g., Coleman, 1961; Harlow, 1994). It is well known that the hydration of ultramafic rocks results in high-pH alkaline fluid (pH ~10) in serpentinites from both orogenic belts and modern seafloor environments (e.g., Coleman, 1971; Kelley et al., 2001). The fluid-inclusion studies of Guatemalan jadeitites (Johnson

TABLE 1. Ion-Probe U-Th-Pb Isotope Data of Zircon in Jadeitite from the Osayama Serpentinite Mélange, Southwest Japan<sup>1</sup>

| Label              | Zone    | U<br>(ppm) | Th<br>(ppm) | p <sub>brad</sub> *<br>(ppm) | *f<br>(%) | Th/U | <sup>238</sup> U/<br><sup>206</sup> Pb | Error | <sup>207</sup> Pb/<br><sup>206</sup> Pb | Error | <sup>207</sup> Pb/<br><sup>206</sup> Pb<br>age**<br>(Ma) | Error |
|--------------------|---------|------------|-------------|------------------------------|-----------|------|--|-------|---|-------|--|-------|
| Grain 01           |         |            |             |                              |           |      |  |       |   |       |  |       |
| #01-1              | Type I  | 11.1       | 2.7         | 0.8                          | 2.23      | 0.25 | 12.00                                  | 4.2   | 0.0686                                  | 10.1  | 509.0  | 21.3  |
| #01-2              | Type I  | 11.7       | 2.4         | 0.7                          | -1.48     | 0.21 | 13.62                                  | 4.0   | 0.0609                                  | 10.8  | 454.2  | 18.2  |
| Grain 05           |         |            |             |                              |           |      |  |       |   |       |  |       |
| #05-11             | Type I  | 15.4       | 3.7         | 1.1                          | -0.96     | 0.25 | 12.21                                  | 3.4   | 0.0660                                  | 8.5   | 502.2  | 16.9  |
| #05-13             | Type I  | 12.5       | 3.4         | 0.8                          | 4.79      | 0.28 | 13.56                                  | 4.1   | 0.0668                                  | 12.4  | 452.8  | 18.8  |
| Grain 07           |         |            |             |                              |           |      |  |       |   |       |  |       |
| #07-34             | Type I  | 21.8       | 6.4         | 1.4                          | -0.78     | 0.30 | 13.13                                  | 3.1   | 0.0603                                  | 8.1   | 471.1  | 14.3  |
| #07-35             | Type I  | 18.2       | 4.9         | 1.3                          | -0.76     | 0.28 | 12.37                                  | 3.1   | 0.0614                                  | 9.6   | 498.7  | 15.8  |
| Grain 09 (Fig. 3A) |         |            |             |                              |           |      |  |       |   |       |  |       |
| #09-15 (3A-3)      | Type I  | 60.4       | 20.5        | 3.9                          | 1.26      | 0.35 | 13.31                                  | 2.2   | 0.0690                                  | 4.9   | 460.0  | 10.3  |
| #09-17 (3A-7)      | Type I  | 46.3       | 14.2        | 3.2                          | 3.15      | 0.32 | 12.26                                  | 2.6   | 0.0748                                  | 8.2   | 494.7  | 13.0  |
| #09-18 (3A-6)      | Type I  | 78.8       | 26.6        | 4.9                          | 0.99      | 0.35 | 13.87                                  | 2.1   | 0.0601                                  | 4.6   | 446.5  | 9.3   |
| #09-19 (3A-5)      | Type I  | 53.2       | 17.4        | 3.4                          | 2.04      | 0.34 | 13.64                                  | 2.3   | 0.0601                                  | 5.6   | 454.0  | 10.6  |
| #09-20 (3A-4)      | Type I  | 58.5       | 19.9        | 3.7                          | 1.12      | 0.35 | 13.58                                  | 2.2   | 0.0602                                  | 5.1   | 455.7  | 10.1  |
| #09-21 (3A-1)      | Type I  | 94.1       | 37.3        | 6.0                          | 0.89      | 0.41 | 13.58                                  | 2.0   | 0.0600                                  | 4.1   | 455.9  | 9.0   |
| #09-22 (3A-2)      | Type I  | 58.8       | 20.1        | 3.8                          | -0.34     | 0.35 | 13.48                                  | 2.3   | 0.0583                                  | 5.4   | 460.2  | 10.4  |
| #09-23 (3A-8)      | Type I  | 81.8       | 29.5        | 5.3                          | 0.69      | 0.37 | 13.36                                  | 2.0   | 0.0593                                  | 4.1   | 463.6  | 9.2   |
| Grain 10           |         |            |             |                              |           |      |  |       |   |       |  |       |
| #10-24             | Type I  | 13.1       | 3.5         | 0.9                          | 4.41      | 0.27 | 12.72                                  | 3.97  | 0.0682                                  | 10.7  | 481.1  | 19.2  |
| #10-27             | Type I  | 11.0       | 2.9         | 0.8                          | -1.22     | 0.27 | 12.21                                  | 3.69  | 0.0692                                  | 9.3   | 500.0  | 18.5  |
| Grain 11 (Fig. 3B) |         |            |             |                              |           |      |  |       |   |       |  |       |
| #11-3              | Type II | 85.2       | 68.0        | 6.3                          | -0.149    | 0.82 | 11.70                                  | 1.89  | 0.0605                                  | 3.5   | 526.9  | 9.8   |
| #11-4              | Type I  | 17.7       | 4.7         | 1.2                          | -0.804    | 0.27 | 12.18                                  | 3.14  | 0.0550                                  | 8.5   | 510.3  | 15.9  |
| #11-5              | Type I  | 17.3       | 3.6         | 1.2                          | -0.897    | 0.21 | 12.52                                  | 3.20  | 0.0659                                  | 8.5   | 490.0  | 15.7  |
| #11-6              | Type I  | 25.4       | 7.5         | 1.6                          | -0.586    | 0.30 | 13.39                                  | 2.86  | 0.0611                                  | 6.8   | 461.5  | 13.1  |
| #11-7              | Type II | 63.5       | 45.0        | 4.3                          | -0.256    | 0.73 | 12.69                                  | 2.12  | 0.0588                                  | 4.7   | 487.7  | 10.2  |
| #11-36             | Type I  | 26.7       | 7.9         | 1.9                          | -0.536    | 0.30 | 11.77                                  | 2.73  | 0.0651                                  | 6.5   | 521.0  | 14.2  |
| Grain 14           |         |            |             |                              |           |      |  |       |   |       |  |       |
| #14-28             | Type I  | 10.4       | 2.2         | 0.7                          | 4.56      | 0.22 | 12.669                                 | 3.94  | 0.0575                                  | 10.3  | 489.4  | 19.2  |
| #14-30             | Type I  | 60.1       | 24.9        | 4.0                          | -0.28     | 0.43 | 12.994                                 | 2.16  | 0.0572                                  | 4.9   | 477.6  | 10.2  |
| #14-31             | Type I  | 46.4       | 21.7        | 3.1                          | -0.37     | 0.48 | 12.853                                 | 2.34  | 0.0633                                  | 5.5   | 479.2  | 11.2  |
| #14-32             | Type I  | 23.1       | 6.5         | 1.5                          | -0.70     | 0.29 | 13.217                                 | 2.93  | 0.0541                                  | 8.0   | 471.5  | 13.7  |
| Grain 15           |         |            |             |                              |           |      |  |       |   |       |  |       |
| #15-37             | Type I  | 26.1       | 7.0         | 1.8                          | -0.52     | 0.28 | 12.204                                 | 2.70  | 0.0613                                  | 6.5   | 505.3  | 13.6  |
| #15-38             | Type II | 83.7       | 61.8        | 5.9                          | 0.39      | 0.76 | 12.210                                 | 1.93  | 0.0596                                  | 3.8   | 506.1  | 9.6   |

<sup>1</sup>All errors are 1  $\sigma$  of standard deviation. \* = percentage of common <sup>206</sup>Pb in total measured <sup>206</sup>Pb. A negative value indicates that the number of ion counts was indistinguishable from background. In such case no common Pb correction is made; \*\* = common Pb correction based on <sup>207</sup>Pb.

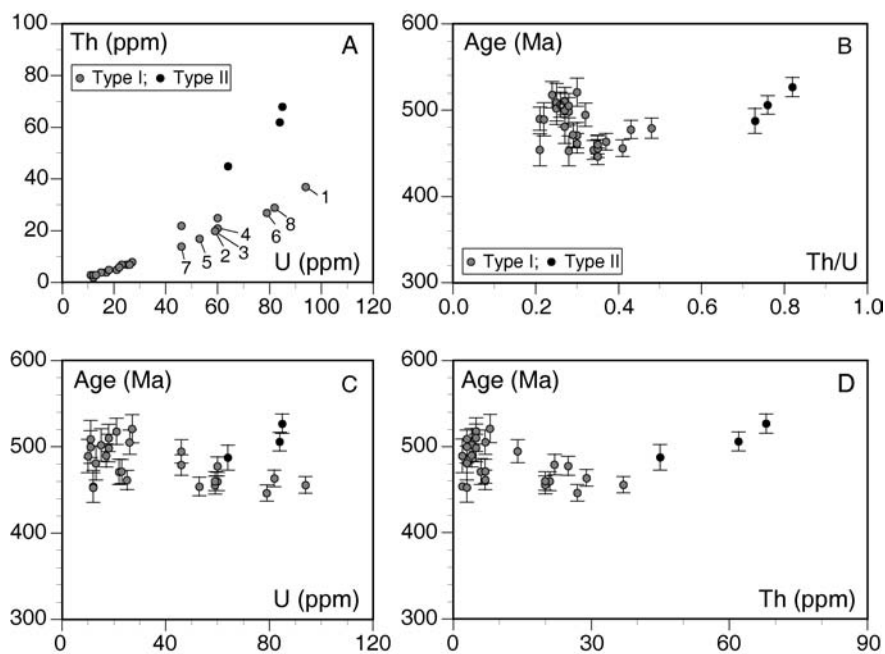


FIG. 5. Plots of apparent  $^{206}\text{Pb}/^{238}\text{U}$  ages (Ma) and Th and U abundance (ppm). Labeled data within plot 5A relate to analyses of zircon shown in Figure 3A. For explanation see text.

and Harlow, 1999) revealed that the infiltration of seawater-like, high-salinity fluid (up to 8 wt% NaCl equivalent) into serpentinites might have played a significant role in jadeitite formation. It is thus possible that serpentinitization and subsequent migration of high-pH, high-salinity fluid in serpentinites were almost contemporaneous. Moreover, some geologic and experimental evidence for Zr mobility in hydrothermal environments indicates that Si-undersaturated fluid containing F, Cl, Na, and Ca can behave as a corrosive solution that promotes high concentrations of high-field-strength elements (HFSEs) (e.g., Hansen and Friderichsen, 1989; Sinha et al., 1992; Vard and Williams-Jones, 1993; Rubatto and Hermann, 2003).

Considering these synthetically, fluid-rock interaction associated with the serpentinitization of ultramafic rocks appears to be the only reasonable process that may account for the Zr concentration and for the precipitation of zircon. Although the source of Zr remains unclear, Zr saturation was most likely supplied by infiltration of an HFSE-enriched subduction-zone fluid or internal source such as clinopyroxene breakdown during serpentinitization, inasmuch as mantle peridotite clinopyroxene con-

tains 10–30 ppm Zr (e.g., Batanova and Sobolev, 2000). In any case, such hydrothermal fluid may have contributed to zircon crystallization during serpentinitization in the subduction-zone environment.

### Time Constraints on Fluid-Rock Interaction

The investigated zircon porphyroblasts have been previously considered as a relict igneous phase (Miyamoto and Yanagi, 1998). Our work has confirmed the result of earlier study that a zircon U-Pb age dated by conventional technique is Ordovician. However, we have also revealed syn-metamorphic, simultaneous growth of zircon with jadeite from the serpentinite-related hydrothermal fluid at a condition of  $P > 1.2$  GPa at  $T < 350^\circ\text{C}$ . Inasmuch as the P-T condition of zircon precipitation is well below the closure temperature of the zircon U-Pb system, we interpret the SHRIMP U-Pb ages as the timing of zircon crystallization from alkaline fluid during the formation of the jadeitite. As mentioned above, the fluid circulation in ultramafic rocks and the subsequent fluid-rock interaction under the LT-HP condition are required to form nearly monomineralic

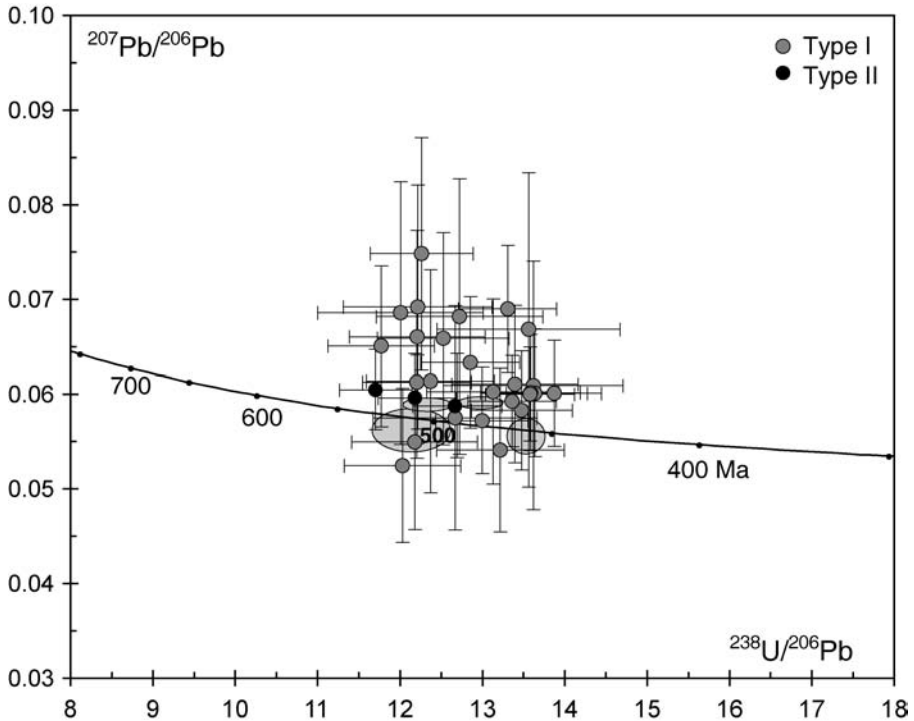


FIG. 6. Tera-Wasserburg diagram for SHRIMP analyses of zircons from the Osayama jadeitite. The grey ellipses represent conventional data by Miyamoto and Yanagi (1998).

jadeitite. Thus, an age of 472 Ma may represent the timing of interaction between hydrothermal fluid and ultramafic rocks in a subduction zone. Fluid circulation may have resulted in varying degrees of metasomatism leading to mineralization of jadeite and zircon during serpentinization. Despite its geologic or tectonic importance, however, radiometric dating of serpentinization is a difficult problem. Although this dating does not provide a direct time constraint for the serpentinization, U-Pb ages of zircon in jadeitite can result in new insights into the minimum age of serpentinization by the fluid-rock interaction of ultramafic rocks at a subduction zone.

The hydrothermal mineralization of 472 Ma is significantly older than the K-Ar ages, 327–273 Ma, of blueschist-facies blocks from the Osayama serpentinite mélangé. This suggests the jadeitite formation is not related to regional Late Paleozoic blueschist-facies metamorphism. In the eastern Chugoku Mountains, Early Paleozoic HP epidote-amphibolites with hornblende K-Ar age of 443–403 Ma occur in a serpentinized peridotite body located

about 180 km to the east of the Osayama serpentinite mélangé (Tsujimori and Liou, 2004b). The jadeitite formation may be related to this Early Paleozoic HP metamorphism.

### Acknowledgments

This research was supported financially in part by JSPS Research Fellowship for Research Abroad of the first author. Preparation of this manuscript and SHRIMP dating was supported by NSF EAR-0003355. We thank R. E. Jones, A. Meibom, J. Hourigan, and R. Y. Zhang for their help in the laboratory, and W. G. Ernst, I. Katayama, G. E. Harlow, and C. G. Mattinson for critical review of an early version of this manuscript.

### REFERENCES

- Arai, S., 1980, Dunite-harzburgite-chromitite complexes as refractory residue in the Sangun-Yamaguchi Zone, western Japan: *Journal of Petrology*, v. 21, p. 141–165.

- Batanova, V. G., and Sobolev, A. V., 2000, Compositional heterogeneity in subduction-related mantle peridotites, Troodos massif, Cyprus: *Geology*, v. 28, p. 55–58.
- Bröcker, M., and Enders, M., 1999, U-Pb zircon geochronology of unusual eclogite-facies rocks from Syros and Tinos (Cyclades, Greece): *Geological Magazine*, v. 136, p. 111–118.
- Cherniak, D. J., and Watson, E. B., 2001, Pb diffusion of zircon: *Chemical Geology*, v. 172, p. 5–24.
- Coleman, R.G., 1961, Jadeite deposits of the Clear Creek area, New Idria district, San Benito County, California: *Journal of Petrology*, v. 2, p. 209–247.
- Coleman, R. G., 1971, Petrologic and geophysical nature of serpentinites: *Geological Society of America, Bulletin*, v. 82, p. 897–918.
- Dubińska, E., Bylina, P., Kozłowski, A., Dörr, W., Nejbort, K., and Schastok, J., 2004, U-Pb dating of serpentinization: Hydrothermal zircon from a metasomatic rodingite shell (Sudetic ophiolite, SW Poland): *Chemical Geology*, v. 203, p. 183–203.
- Erlank, A. J., Smith, A. S., Marchant, J. W., Cardoso, M. P., and Ahrens, L. H., 1978, *Zr*, in Wedepohl, K. H., ed., *Handbook of geochemistry*, v. II-4, section 40: New York, NY, Springer.
- Harlow, G. E., 1994, Jadeitites, albitites and related rocks from the Motagua Fault Zone, Guatemala: *Journal of Metamorphic Geology*, v. 12, p. 49–68.
- Hansen, B. T., and Friderichsen, J. D., 1989, The influence of recent Pb-loss on the interpretation of disturbed U-Pb systems in zircons from igneous rocks in East Greenland: *Lithos*, v. 23, p. 209–223.
- Hayasaka, Y., Sugimoto, T., and Kano, T., 1995, Ophiolitic complex and metamorphic rocks in the Niimi-Katsuyama area, Okayama Prefecture: Excursion Guidebook of 102nd Annual Meeting of the Geological Society of Japan, p. 71–87 (in Japanese).
- Hoskin, P. W. O., 2000, Patterns of chaos: Fractal statistics and the oscillatory chemistry of zircon: *Geochimica et Cosmochimica Acta*, v. 64, p. 1905–1923.
- Ishiwatari, A., and Tsujimori, T., 2003, Paleozoic ophiolites and blueschists in Japan and Russian Primorye in the tectonic framework of East Asia: A synthesis: *The Island Arc*, v. 12, p. 190–206.
- Isozaki, Y., 1996, Anatomy and genesis of a subduction-related orogen: A new view of geotectonic subdivision and evolution of the Japanese Island: *The Island Arc*, v. 5, p. 289–320.
- Johnson, C. A., and Harlow, G. E., 1999, Guatemala jadeitites and albitites were formed by deuterium-rich serpentinizing fluids deep within a subduction-channel: *Geology*, v. 27, p. 629–632.
- Kelley, D. S., Karson, J. A., Blackman, D. K., Fruh-Green, G. L., Butterfeld, D. A., Lilley, M. D., Olson, E. J., Schrenk, M. O., Roe, K. V., Lebonk, G. T., Rivizzigno, P., and the AT3-60 Shipboard Party, 2001, An off-axis hydrothermal vent field near the Mid-Atlantic Ridge at 30°N: *Nature*, v. 412, p. 145–149.
- Katayama, I., Mukou, A., Iizuka, T., Maruyam, S., Terada, K., Tsutsumi, Y., Sano, Y., Zhang, R. Y., and Liou, J. G., 2003, Dating of zircon from Ti-clinohumite-bearing garnet peridotite: Implication for timing of mantle metasomatism: *Geology*, v. 31, p. 713–716.
- Kobayashi, S., Miyake, H., and Shoji, T., 1987, A jadeite rock from Oosa-cho, Okayama Prefecture, southwestern Japan: *Mineralogical Journal*, v. 13, p. 314–327.
- Kunugiza, K., Nakamura, E., Miyajima, H., Goto, A., and Kobayashi, K., 2002, Formation of jadeite-natrolite rocks in the Itoigawa-Ohmi area of the Hida marginal belt inferred from U-Pb zircon dating: 2002 Joint Annual Meeting of The Japanese Association of Mineralogists, Petrologists, and Economic Geologists, and The Mineral Society of Japan, Abstracts (in Japanese).
- Ludwig, K. R., 2001, SQUID 1.02: Berkeley, CA, Berkeley Geochronology Center, Special Publication no. 2.
- Ludwig, K. R., 2003, Isoplot 3: Berkeley, CA, Berkeley Geochronology Center, Special Publication, no. 4.
- Miyajima, H., Matsubara, S., Miyawaki, R., and Hirokawa, K., 2001, Rengeite, Sr<sub>4</sub>ZrTi<sub>4</sub>Si<sub>4</sub>O<sub>22</sub>, a new mineral, the Sr-Zr analogue of perrierite from the Itoigawa-Ohmi district, Niigata Prefecture, central Japan: *Mineralogical Magazine*, v. 65, p. 111–120.
- Miyamoto, T., and Yanagi, T., 1998, U-Pb dating of zircon in jadeite rock in Oosayama serpentinite melange from Okayama Pref., Southwest Japan: 1998 Joint Annual Meeting of the Japanese Association of Mineralogists, Petrologists, and Economic Geologists, and The Mineral Society of Japan, Abstract, p. 190 (in Japanese).
- Powell, R., Holland, T. J. B., and Worley, B., 1998, Calculating phase diagrams involving solid solutions via non-linear equations, with examples using THERMOCALC: *Journal of Metamorphic Geology*, v. 16, p. 577–588.
- Rubatto, D., and Hermann, J., 2003, Zircon formation during fluid circulation in eclogites (Monviso, Western Alps): Implications for Zr and Hf budget in subduction zones: *Geochimica et Cosmochimica Acta*, v. 67, p. 2173–2187.
- Rubin, J. N., Henry, C. D., and Prince, J. G., 1989, Hydrothermal zircons and zircon overgrowths, Sierra Blanca Peaks, Texas: *American Mineralogist*, v. 74, p. 865–869.
- Sinha, A. K., Wayne, D. M., and Hewitt, D. A., 1992, The hydrothermal stability of zircon: Preliminary experimental and isotopic studies: *Geochimica et Cosmochimica Acta*, v. 56, p. 3551–3560.
- Shi, G. H., Cui, W. Y., Tropper, P., Wang, C. Q., Shu, G. M., and Yu, H., 2003, The petrology of a complex sodic and sodic-calcic amphibole association and its implications for the metasomatic processes in the jadeite area in northwestern Myanmar, formerly Burma: *Contributions to Mineralogy and Petrology*, v. 145, p. 355–376.
- Shoji, T., and Kobayashi, S., 1988, Fluid inclusions found in jadeite and stromalolite, and a comment on the

- jadeite-analcime boundary: *Journal of Mineralogy, Petrology, and Economic Geology*, v. 83, p. 1–8.
- Tsujimori, T., 1997, Omphacite-diopside vein in an omphacitite block from the Osayama serpentinite melange, Sangun-Renge metamorphic belt, southwestern Japan: *Mineralogical Magazine*, v. 61, p. 845–852.
- Tsujimori, T., 1998, Geology of the Osayama serpentinite melange in the central Chugoku Mountains, southwestern Japan: 320 Ma blueschist-bearing serpentinite melange beneath the Oeyama ophiolite: *Journal of the Geological Society of Japan*, v. 104, p. 213–231 (in Japanese with English abstract).
- Tsujimori, T., and Itaya, T., 1999, Blueschist-facies metamorphism during Paleozoic orogeny in southwestern Japan: Phengite K-Ar ages of blueschist-facies tectonic blocks in a serpentinite melange beneath Early Paleozoic Oeyama ophiolite: *The Island Arc*, v. 8, p. 190–205.
- Tsujimori, T. and Liou, J. G., 2004a, Coexisting chromian omphacite and diopside in tremolite schist from the Chugoku Mountains, SW Japan: The effect of Cr on the omphacite-diopside immiscibility gap: *American Mineralogist*, v. 89, p. 7–14.
- Tsujimori, T., and Liou, J. G., 2004b, Metamorphic evolution of kyanite-staurolite-bearing epidote-amphibolitic rocks from the Early Paleozoic Oeyama belt, SW Japan: *Journal of Metamorphic Geology*, v. 22, p. 301–313.
- Tsujimori, T., and Liou, J. G., 2005a, Eclogite-facies mineral inclusions in clinozoisite from Paleozoic blueschist, central Chugoku Mountains, SW Japan: Evidence of regional eclogite-facies metamorphism: *International Geology Review*, v. 47, p. 215–232.
- Tsujimori, T., and Liou, J. G., 2005b, Low-pressure and -temperature K-bearing kosmochloric diopside from the Osayama serpentinite mélange, SW Japan: *American Mineralogist*, v. 90, in press.
- Vard, E., and William-Jones, A. E., 1993, A fluid inclusion study of vug minerals in dawsonite phonolite sills, Montreal, Quebec: Implications for HFSE mobility: *Contributions to Mineralogy and Petrology*, v. 113, p. 410–423.
- Vavra, G., Schmid, R., and Gebauer, D., 1999, Internal morphology, habit and U-Th-Pb microanalysis of amphibolite-to-granulite facies zircons: Geochronology of the Ivrea zone (Southern Alps): *Contributions to Mineralogy and Petrology*, v. 134, p. 380–404.
- Williams, I. S., 1998, U-Th-Pb geochronology by ion microprobe, in Mickibbeen, M. A., Shanks, W. C., III, and Ridley, W. L., eds., *Application of microanalytical techniques to understanding mineralizing processes*: Society of Economic Geology, *Reviews in Economic Geology*, v. 7, p. 1–35.